MULTISCALE SIMULATION OF THE COMPETITION BETWEEN TRANSGRANULAR AND INTERGRANULAR DUCTILE FRACTURE

F. Scheyvaerts[1], P.R. Onck[2], Y. Bréchet[3] and T. Pardoen[1].

[1]Département des Sciences des Matériaux et des Procédés, Université catholique de Louvain, IMAP, Belgium;

[2] Department of Applied Physics, University of Groningen, Micromechanics of Materials, The Netherlands;

[3] Laboratoire de Thermodynamique et Physico-chimie Métallurgiques, ENSEEG, Institut National Polytechnique de Grenoble, France.

ABSTRACT

The competition between intergranular and transgranular fracture in aluminium alloys with precipitate free zones (PFZs) along grain boundaries is investigated using a multiscale approach. Ductile fracture occurs both in the grains and in the soft PFZ through the nucleation of voids at second phase inclusions, their growth and subsequent coalescence. A grain level unit cell model has been developed in order to capture the link between the microstructure, the flow properties and the ductility, which is very much dictated by the inter- vs. transgranular mode of cracking. The constitutive description used in both regions is an extension of the Gurson model, accounting for void shape effects, void rotation and hardening. When the yield stress in the interior of the grains is high (resp. low), the fracture is purely intergranular (resp. transgranular). For intermediate yield stress, part of the fracture is intergranular and part of the fracture is transgranular. It is also shown that the elongation of the grain in the principal loading direction (resp. in the transverse direction) favours transgranular (resp. intergranular) mode of failure.

1 INTRODUCTION

In some materials, spatial heterogeneities in mechanical properties and microstructural features are responsible for the coexistence of different ductile failure modes, such as in multiphase materials involving several ductile phases. In particular, in some aluminium alloys, the microstructure consists of precipitate free zone along the gain boundary with large second phase inclusions, and a precipitation hardened state within the grain. The failure mode of the material can be either intragranular or intergranular ductile fracture, or a combination of the two, see [1,2].

A schematic of the microstructure is shown in Fig. 1a. The individual features controlling the fracture of aluminium alloys are well identified. They indicate the relevant parameters to be introduced in our micromechanical model. The influence of the heat treatments will be lumped into an evolution of the yield stress and work hardening. The grain interior after heat treatment will have a high yield stress σ_{0g} and a low work hardening rate n_g. On the other hand, the PFZ will have a low yield stress σ_{0p} and a high work hardening rate n_p. The idealised microstructure is shown in Fig. 1b with the various length scales entering the problem. The relevant dimensionless quantities which will appear in the model, together with the mechanical properties, are given in Fig. 1c : the relative PFZ thickness R, the void volume fraction f, the void aspect ratio W, the void distribution factor λ, the Young's modulus E, the Poisson ratio ν, the yield stress $\sigma_{0(i)}$, and the strain-hardening exponent $n_{(i)}$ (the subscript (i) stands for either "p", i.e. precipitate free zone (PFZ) or "g", i.e. grain interior. A subscript "0" will be added when referring to the initial state). The density and initial size of the cavities will be considered uniform inside the grain and the PFZ. The uniaxial elastic/plastic tensile behaviour of the matrix material in the grain interior and the PFZ is described by a simple two-parameter description for the matrix stress σ_M and strain ε_M:
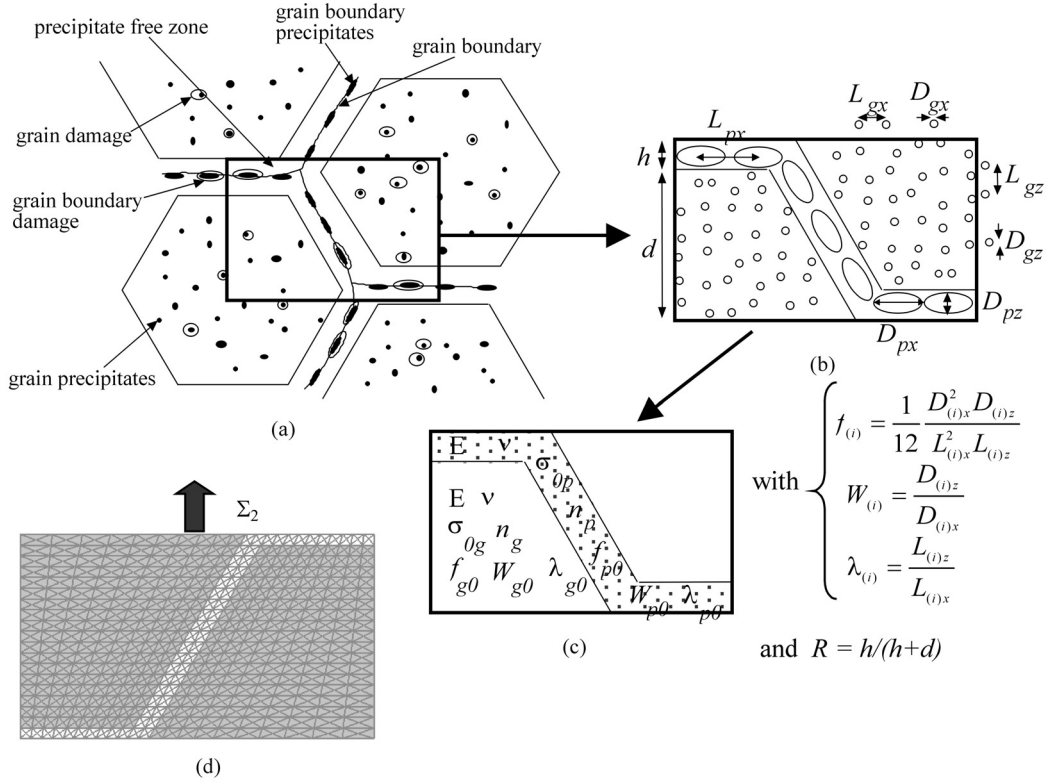
Figure 1: Description of (a) a realistic model of the microstructure and failure mechanisms, of (b) the idealised microstructure, of (c) the continuum micromechanical model and of (d) the finite element unit-cell used for the analysis.

$$\frac{\sigma_M}{\sigma_0} = \frac{E\varepsilon_M}{\sigma_0} \qquad \text{when} \quad \sigma_M < \sigma_0, \qquad\qquad (1)$$

$$\frac{\sigma_M}{\sigma_0} = \left(1 + \frac{E\varepsilon_M}{\sigma_0}\right)^n \qquad \text{when} \quad \sigma_M > \sigma_0, \qquad\qquad (2)$$

where the subscripts (i) are omitted for clarity.

   In the present paper the aim is to establish which mode dominates as a function of the yield stress and grain shape mismatches. Indeed, in 7000 aluminium alloys, the yield stress of the grain interior is the parameter that can most easily be modified experimentally by proper ageing treatment [1]. Furthermore, non equiaxed grain shapes are always produced by the rolling process. Such a quantitative analysis of this highly non-linear problem of failure mode transition requires a detailed model for ductile damage to be incorporated in both the PFZ and the grain interior. The material model used here is an elastic-viscoplastic continuum model for the growth and coalescence of spheroidal voids. The model will be used for both areas, only accounting for a difference in mechanical properties and microstructure as shown in Fig. 1c.

2 CONSTITUTIVE MODEL FOR DUCTILE DAMAGE

2.1 The void growth stage

Pardoen and Hutchinson [3] have developed a Gurson-type void growth model [4] that describes the plastic flow in a continuous porous medium. The model extends the contribution of Gologanu-Leblond-Devaux [5] to strain hardening. It is a full constitutive model for a porous elastoplastic material containing spheroidal voids. The model contains nine state variables: the six components of the mesoscopic stress tensor $\boldsymbol{\Sigma}$, the porosity f, the void aspect ratio S, and the average yield stress of the matrix material σ_M. The void aspect ratio is defined by $S = \ln(W)$.

The equations of the void growth model are :

$$\Phi \equiv \Phi(\boldsymbol{\Sigma}, f, S, \sigma_M) = 0 , \tag{3}$$

$$\dot{f} = (1 - f) tr(\dot{\boldsymbol{\eta}}^{\mathbf{p}}) , \tag{4}$$

$$\dot{S} \equiv \dot{S}(f, S, T) , \tag{5}$$

$$\sigma_M \dot{\varepsilon}_M^p (1 - f) = \boldsymbol{\Sigma} : \dot{\boldsymbol{\eta}}^{\mathbf{p}} , \tag{6}$$

$$\dot{\boldsymbol{\eta}}^{\mathbf{p}} = \Lambda \frac{\partial \Phi}{\partial \boldsymbol{\Sigma}} , \tag{7}$$

$$\dot{\varepsilon}_M^p \equiv \dot{\varepsilon}_M^p (\sigma_M) , \tag{8}$$

where Φ is the flow potential; $\dot{\boldsymbol{\eta}}^{\mathbf{p}}$ is the mesoscopic plastic strain tensor; eqns (4) and (5) are the evolution laws for f and S, respectively; T is the stress triaxiality defined as $T = \Sigma_{hh}/3\Sigma_e$, and Σ_e is the effective stress; eqn (6) is the energy balance for the plastic work allowing computation of σ_M (see [4]) using the effective stress-strain curve for the parent material (2); and eqn (7) is the flow rule. Strain rate sensitivity is included in the model by taking the response of the matrix material to be elastic-viscoplastic. The hardening matrix material is assumed to follow a power law relation in addition to elasticity. The plastic part of the Lagrangian strain rate is given by (8).

2.2 Void coalescence

The coalescence model, derived from Thomason's criterion for the onset of coalescence [6], directly addresses the mechanism of tensile plastic localization in the ligaments between neighbouring voids, leading to a uniaxial mode of straining. The criterion of Thomason has been extended to strain-hardening materials in [3]. In order to couple the coalescence model with the void growth model (2) to (8), a new state variable related to the void distribution, $\chi = R_X / L_X$ (where R is the void radius), has been introduced. Coalescence occurs when the stress component in the direction of the void axis reaches a critical value:

$$\sigma_n \equiv \boldsymbol{\sigma} : (\hat{\mathbf{e}}_{\mathbf{z}} \otimes \hat{\mathbf{e}}_{\mathbf{z}}) = (1 - \chi^2) \left[\alpha \left(\frac{1 - \chi}{\chi W^2} \right) + \beta \sqrt{\frac{1}{\chi}} \right], \tag{9}$$

where $\hat{\mathbf{e}}_{\mathbf{z}}$ is the base vector of the reference system attached to the void that is aligned with the main void axis; the parameter α is given by the fit (for $0 \leq n \leq 0.3$) $\alpha = 0.1 + 0.217n + 4.83n^2$,

while β can be considered as constant and equal to 1.24. Once criterion (9) is met, further straining develops uniaxially in the direction of the void axis:

$$\dot{\boldsymbol{\eta}}^{C} = \dot{\varepsilon}_{n}^{C}(\hat{\mathbf{e}}_{\mathbf{z}} \otimes \hat{\mathbf{e}}_{\mathbf{z}}), \tag{10}$$

where the normal strain rate is given by a power law relation similar to (8) but with a linear decrease of σ_n with increasing ε_n^p. Finite element void cell calculations are used to tabulate the unloading slopes as a function of the stress triaxiality, the void shape and the relative position of neighbouring voids (e.g. [3]).

The total strain rate tensor $\dot{\boldsymbol{\eta}}$ is decomposed in an elastic part $\dot{\boldsymbol{\eta}}^{E}$ and a viscoplastic part $\dot{\boldsymbol{\eta}}^{VP}$. The elastic response is governed by the hypo-elastic relationship

$$\overset{\triangledown}{\boldsymbol{\sigma}} = \mathbf{R} : \dot{\boldsymbol{\eta}}^{E} = \mathbf{R} : (\dot{\boldsymbol{\eta}} - \dot{\boldsymbol{\eta}}^{VP}), \tag{12}$$

in terms of the Jaumann stress-rate $\overset{\triangledown}{\boldsymbol{\sigma}} = \dot{\boldsymbol{\sigma}} - \mathbf{W} \cdot \boldsymbol{\sigma} + \boldsymbol{\sigma} \cdot \mathbf{W}$ ($\mathbf{W}$ is the skew symmetric part of the velocity gradient tensor $\mathbf{L}$). The fourth-order modulus tensor $\mathbf{R}$ is expressed in the usual way in terms of Young's modulus E and Poisson's ratio ν. During void growth, the viscoplastic strain rate is determined by eq. (7), $\dot{\boldsymbol{\eta}}^{VP} = \dot{\boldsymbol{\eta}}^{P}$. When the coalescence criterion (9) is met, further straining is described by eq. (10), using $\dot{\boldsymbol{\eta}}^{VP} = \dot{\boldsymbol{\eta}}^{C}$.

3 RESULTS OF SIMULATIONS ON A SINGLE GRAIN CELL WITH PERIODIC BOUNDARY CONDITIONS

The constitutive model presented in the previous section is analyzed using an incremental finite strain, finite element method. A plane strain, total Lagrangian, convected coordinate formulation is used [7]. We analyze an infinitely large polycrystalline aggregate consisting of hexagonal grains (see Fig. 1), from which a unit cell can be identified. The material is subjected to uniaxial tension in the vertical direction (Σ_l=0). Fig. 1d shows the finite element mesh used, accounting for the symmetry of the problem. Each quadrilateral element is built up of four constant strain triangles. To ensure symmetry of the unit-cell during loading the edges of the unit-cell are constrained to remain straight. This is achieved by using a Rayleigh-Ritz technique that controls the normal displacement rates, such that the stress ratio, Σ_l/Σ_2, remains zero.

The competition between hardening and void softening in the PFZ is primarily driven by the flow properties of the grain with respect to the flow properties of the PFZ. The deformation of the two material parts is described by the constitutive model presented in section 2. The microstructural and micromechanical parameters of the model, summarised in Fig. 1, are given the following values for typical 7000 aluminium alloys [1] : $f_{g0} = 10^{-3}$, $n_g = 0.05$, $W_{g0} = 1$, $\lambda_{g0} = 1$, $f_{p0} = 2.5\ 10^{-2}$, $n_p = 0.3$, $W_{p0} = 1$, $\lambda_{p0} = 1$, $\sigma_{0p}/E = 10^{-3}$, $R_0 = 0.1$.

The key ingredients of the flow behaviour chosen are a PFZ softer than the grain interior, but presenting an enhanced work hardening rate [2]. The elastic constants are the same in both layers :

$$\nu_g = \nu_p = \nu = 0.35 \qquad \text{and} \qquad E_g = E_p = E.$$

The PFZ yield stress, specified through the ratio σ_{0g}/σ_{0p}, will take distinct values. Fig. 2 presents the overall stress-strain curves. The saw-tooth shape of the stress-strain curve during the coalescence phase in Fig. 2 shows that the microstructure is fractured progressively during

deformation. This is a consequence of the size of the unit cell being too small to capture adequately the average behaviour of a random representative material element. A larger unit-cell with random grains is necessary to reproduce a more realistic polycrystalline response.

The sequence of fracture events is also shown for three yield stress ratii, 4, 6 and 8, through a chronological serie of numbers on the right hand side of Fig. 2. The transition from intergranular (σ_{0g}/σ_{0p}=8) to transgranular failure (σ_{0g}/σ_{0p}=4) is captured. A yield stress ratio equal to 6 gives an intermediate situation, where damage initiated at the triple grain junctions spreads at the same time in the grain and along the boundaries. So, as expected from [2], an increase of the grain yield stress promotes grain boundary failure. On Fig. 3, the transition is displayed by a significant drop of ductility with the yield stress ratio.

Similar calculations have been performed with grains elongated while loading is applied either in the longitudinal direction (W_G=6) or in the transverse direction (W_G=1/6). The PFZ thickness is kept constant. When the grain aspect ratio W_G is large, the transgranular mode of failure is favoured in the full range of σ_{0g}/σ_{0p} considered here. Indeed most of the PFZ is aligned perpendicularly to the principal loading direction. Constraint effect cannot play a major role. The grain and the aligned PFZ undergo more or less the same strain. The crack first initiated in the small transverse PFZ creates a stress concentration in the grain and propagate straight. On the other hand, if the principal loading is transverse to the large grain diameter, crack propagates easily along the soft grain boundaries, and the mode of failure is intergranular for the whole range of yield stress ratio. Nevertheless, if prolate grain (W_G=6) gives larger ductility (see Fig. 3), the effect of grain shape is only very significant at large yield stress mismatch when compared to oblate one (W_G=1/6). Note that calculations for larger stress triaxialities (T=1 and T=3) show a dominant intergranular mode of failure for the three grain shapes.
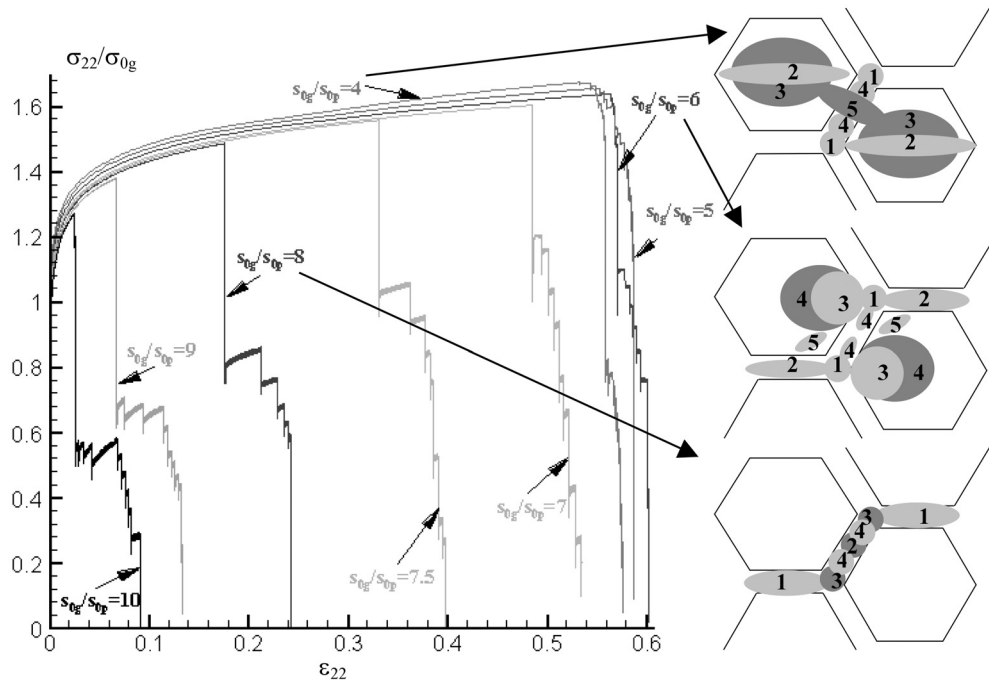

Figure 2: Macroscopic flow curves and corresponding cracks path for different values of the yield stress ratio between the grain and the PFZ.
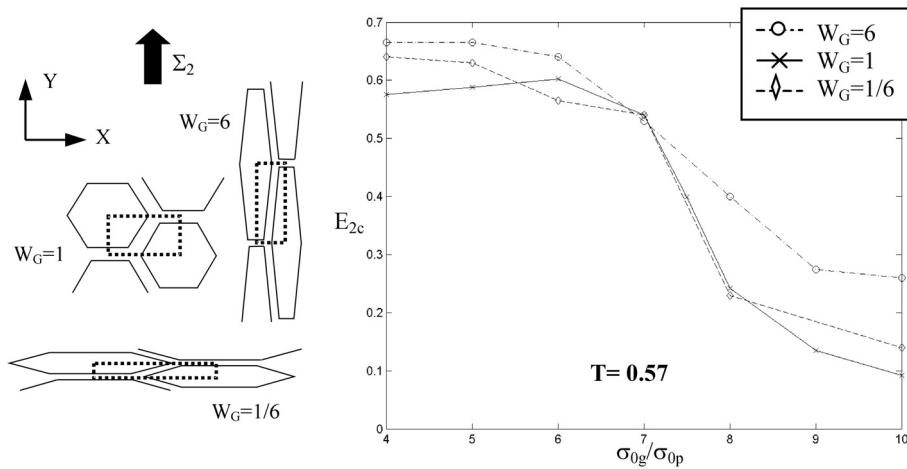
Figure 3: Evolution of the final strain at failure with the yield stress ratio for 3 distinct values of the grain shape, at T=0.57.

4 CONCLUSION AND PERSPECTIVES

A multiscale model featuring a soft and a hard damaging zone has been developed in order to elucidate the competition between grain boundary and transgranular failure in aluminium alloys. As a first prediction, a higher grain yield stress increases the risk of grain boundary failure within the precipitate free zone (PFZ), which is consistent with experimental measurements performed on 7040 and 7050 alloys [1]. On the other hand, increasing the triaxiality or loading in the direction tranverse to elongated grains favours intergranular failure. An important aspect of the present micromechanical model is that it accounts for the effective shear on void growth and coalescence, which is essential for modelling the response of PFZ not aligned with the principal strain direction. The next step in this study is to move to polycrystal aggregates in order to simulate realistic volume elements as well as capturing details of the crack propagation mechanisms.

REFERENCES

1. Dumont, D., Deschamps, A. and Brechet, Y., *Materials Science and Engineering*, Vol. 356, 326-336, 2003.

2. Pardoen, T. *et al.*, *Journal of the Mechanics and Physics of Solids*, Vol. 51, 637-665, 2003.

3. Pardoen, T. and Hutchinson, J.W., *Journal of the Mechanics and Physics of Solids*, Vol. 48, 2467-2512, 2000.

4. Gurson, A.L., *Journal of Engineering Materials and Technology*, Vol. 99, 2-15, 1977.

5. Gologanu, M. *et al.*, In *Suquet, P. (Ed.) Continuum Micromechanics*, Springer-Verlag, 1995.

6. Thomason, P.F., *Ductile Fracture of Metals*, Pergamon Press, Oxford, 1990.

7. Tvergaard, V., *Advances in applied Mechanics*, Vol. 27, 83-151, 1990.

8. Onck, P.R. and Van der Giessen, E., *Journal of the Mechanics and Physics of Solids*, Vol. 47, 99-139, 1999.